Orientational order in gravity dispersed clay colloids: A synchrotron x-ray scattering study of Na fluorohectorite suspensions

E. DiMasi,[1,*] J. O. Fossum,[2] T. Gog,[3] and C. Venkataraman[3]
[1]*Physics Department, Brookhaven National Laboratory, Upton, New York 11973-5000*
[2]*Department of Physics, Norwegian University of Science and Technology, N-7491 Trondheim, Norway*
[3]*CMC-CAT, Advanced Photon Source, Argonne National Laboratory, Argonne Illinois 60439*
(Received 5 June 2001; published 21 November 2001)

Colloidal suspensions of clay particles in aqueous salt solutions make ideal model systems for the study of interactions between plate-shaped particles, due to the ease in tuning their electrostatic repulsion with the concentration of the salt. Numerous gel and sol structures are possible, including nematic liquid crystalline order, although only qualitative identification of the latter in clay colloids has been available so far. We present synchrotron x-ray diffraction from gravity dispersed solutions of Na fluorohectorite, a synthetic swelling clay, over a large NaCl concentration range. Our use of liquid scattering techniques allows us to identify regions in which particles reorient from horizontal to vertical alignments in strata coexisting at different heights within the sample. We identify two distinct gel regions characterized by differences in orientational anisotropy and domain size. Our results provide direct evidence for nematic order, as well as unique structural information regarding particle morphology and alignment within each of the colloid phases.

DOI: 10.1103/PhysRevE.64.061704 PACS number(s): 61.10.−i, 61.30.Eb

I. INTRODUCTION

Clay particles dispersed in salt solutions have been studied for decades, in part to learn how to control technologically important clay suspensions, and in part because they are diverse, tunable examples of plate-shaped colloidal particles [1]. The versatility of clays comes from their layered microstructure and platelet morphology. The individual particles are composed of one or more silicate lamellae that stack by sharing exchangeable cations between their faces [Figs. 1(a) and 1(b)]. Although the layered subunit is crystalline, relative registry and orientations between lamellae are usually quite disordered. Substitution of metals either within the silicate layer or at the exchangeable cation site produces a surface charge that affects the absorption of water into the interlayer space, and hence controls the layer spacing [2]. These features determine a net negative surface charge for the particle, and in combination with the particle size and the interactions with the screening salt in solution, produce wonderfully rich phase behavior in the clay suspensions [3,4].

The complexity arises from the several ways in which attractive and repulsive forces may play out. When van der Waals attraction between the particles is balanced by electrostatic repulsion, particles can remain dispersed, settling only slowly out of solution. Ions from an electrolyte, if present, can screen the repulsive forces between particles and allow them to aggregate together. This aggregation or ''flocculation,'' may cause the particles to quickly settle out of suspension. On the other hand, attracted particles may join to form extended networks, resulting in gels. Because the particles will, in general, have a negative surface charge partly compensated by positive charge at the particle edges, it is surmised that the particles are connected in edge-to-face configurations [Fig. 1(c)]: the result is an isotropic, so-called ''house of cards'' structure that has inspired many theoretical investigations [5], although most recent experimental work has failed to support this model.

Perhaps the most interesting structural correlations that may be expected are those of liquid crystal phases. There has been particular interest in nematic phases, which would exhibit parallel orientation of the platelets but have no long-range positional order [6]. If the system is made dense enough, it becomes favorable for particles to align, giving up orientational entropy in exchange for much greater positional entropy. Thus, in plate colloid systems, a transition from an isotropic to a nematic phase is expected at a critical particle density [7]. The salt concentration plays a subtle role here in addition to determining the overall magnitude of repulsive forces, because the spatial extent of electrical diffuse layers modifies the effective anisotropy of the interacting particles [8].

Understanding the role of salt in stabilizing dense clay phases can have practical significance. For example, ''quick-clay'' soils composed of illite particles, originally sedimented in salt water, can be progressively destabilized by subsequent

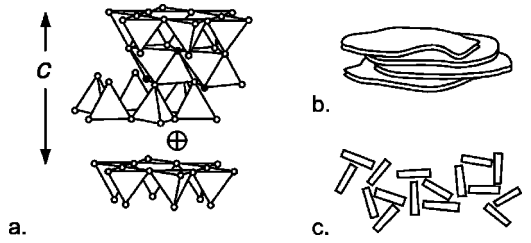

FIG. 1. (a) Generic smectite structure showing oxygen (○), fluorine (●), and exchangeable cation (⊕) sites (after Ref. [2]). (b) Micron-scale clay particle formed from stacked lamellae. (c) Face-to-edge and edge-to-edge aggregation of clay particles.

*Author to whom correspondence should be addressed. Electronic address: dimasi@bnl.gov

fresh-water rinsing: here, the consequence of reduced salt concentration is literally a sinkhole or landslide. Much effort has gone into relating the structural and rheological properties of clay-salt suspensions to optical observations, which find birefringent domains with defect textures characteristic of nematic liquid crystals [3,4,9]. Small-angle neutron scattering measurements have also suggested the presence of local orientational correlations in smectite clay gels [10]. Direct *in situ* structural evidence for parallel alignment of platelets, however, has not been obtained.

In this paper, we describe suspensions of the synthetic 2:1 smectite clay Na fluorohectorite (Na-Fh) in aqueous NaCl solutions. Like natural hectorite, Na-Fh is a swelling clay that incorporates a variable amount of water in the interlayer space, resulting in a change in lattice constant along the stacking direction. Na-Fh has a rather large surface charge of 1.2 *e* /unit cell, compared, for example, to other synthetic smectites such as laponite (0.4 *e* /unit cell) [11]. Na-Fh also has a quite large and variable particle size of up to 20 000 Å in diameter, and compared to natural clays such as montmorillonite, might be expected to have a more homogeneous composition and charge distribution. The polydispersity in particle size makes the Na-Fh suspensions particularly interesting, because gravitational forces effectively sort the particles by size, stabilizing in some cases several strata of gels, sols and/or sediments within a single sample tube [12,13]. The strong influence of polydispersity in particle size and aspect ratio on the phase diagram of plate colloids is the focus of numerous recent articles [14–17].

Our aim is to learn about the structural correlations in this system, and, in particular, conduct synchrotron x-ray scattering experiments that are sensitive to the orientation of the particles. For example, edge-to-face flocculation would result in random orientation of the particles, while in a nematic liquid crystalline phase, the platelets would be parallel to each other. Because the sample tubes cannot be tilted in the x-ray beam without disturbing the boundaries between the strata, we have made use of a specialized spectrometer designed for the study of liquid surfaces [18]. It is worth pointing out that while some basic information is available on the structure and hydration behavior of this clay [11], a complete investigation of the crystallography remains to be done. In interpreting the diffraction patterns in this work, we rely on our own studies in progress on powder diffraction from dry Na-Fh [19] and temperature- and humidity-dependent diffraction from partially oriented pressed samples [20], along with the available published literature [11].

II. EXPERIMENTAL METHODS

Fluorohectorite clay was purchased from Corning [21] and ion exchanged through dialysis to produce Na-fluorohectorite having the nominal chemical formula $Na_{0.6}Mg_{2.4}Li_{0.6}Si_4O_{10}F_2$. Solutions were prepared having 2.91–2.94 wt % clay in NaCl concentrations ranging from 1.0×10^{-4} to $1.2\times10^{-2}M$. X-ray scattering measurements were carried out using the CMC-CAT liquid surface spectrometer at beamline 9ID-C at the Advanced Photon Source. Using the third harmonic of the undulator, the x-rays were monochromatized at 19 keV, or an x-ray wavelength of 0.653 Å. Incident slits restricted the beam spot size to 0.4 $\times$0.4 mm^2. The instrumental resolution was determined principally by 0.5$\times$0.5 mm^2 slits before the NaI single channel detector, 600 mm from the sample.

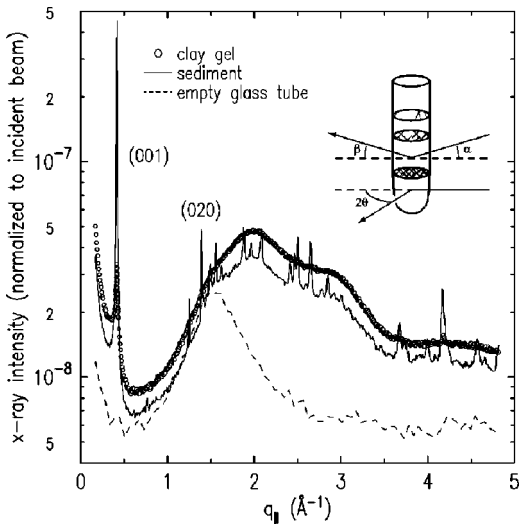

FIG. 2. X-ray scattering pattern of clay gel (○) and sediment (—) strata. Powder peaks from the clay particles are superimposed on the bulk structure factors of glass (- - -) and water. Inset: scattering geometries parallel and perpendicular to the strata in the sample tube. Angles α and β are defined relative to the horizontal plane. The scattering angle 2θ is relative to the path of the direct beam through the sample.

A few days before the x-ray experiments, the suspensions were shaken thoroughly and poured from their original containers into glass tubes $\approx$8 mm in diameter, with wall thicknesses of 0.2–0.3 mm. In some cases, water had evaporated from the original mixtures, increasing the NaCl concentration by up to 5% from the nominal one. Since the experiments on each sample took from one to two days, the last samples studied had a week or more to settle, while those measured first had been sitting only for a few days after being remixed. This was enough time for the strata to stabilize, as judged by boundaries visible to the eye that remained at a fixed height. However, some of our x-ray results suggest that settling or gellation was still occurring within these strata on some samples. Unless noted otherwise, we present here results only from samples that seemed to be stable on the scale of ten hours or so. All samples were reexamined five months later, and at this time the gel regions took up much less volume than in our x-ray study, with much larger volumes of clear liquid at the tops of the tubes. Clearly, a complete characterization of the system will require additional studies of samples mixed in their x-ray holders and allowed to relax for considerably longer times.

Different strata within each sample tube were positioned in the beam by means of an elevator stage. Since the beam was 0.4 mm in height, we typically took sample height steps of 0.5 mm or larger. We made measurements in two different scattering geometries, as shown in the inset of Fig. 2. With a level incoming beam (parallel to the strata, with $\alpha=\beta=0$), momentum transfer in the horizontal plane is a function of

scattering angle 2θ around a vertical axis: $q_{\|} = (4\pi/\lambda)\sin(2\theta/2)$. Momentum transfer along the vertical direction is achieved by tilting the beam down at an angle α to the strata, while detecting x-rays scattered upwards at angle β, with $2\theta = 0$: $q_{\perp} = (2\pi/\lambda)(\sin\alpha + \sin\beta)$. By measuring intensities of $(00L)$ Bragg peaks in both geometries, we can determine the relative populations of clay platelets in two orientations: horizontal (those lying parallel to the strata, as if flat on the floor) and vertical (as if standing upright on edge).

III. EXPERIMENTAL RESULTS

A. Peak positions and line shapes

The positions and line shapes of the peaks provide specific information about the clay particles' structure and morphology. Scattered intensity as a function of $q_{\|}$ at several heights within one sample tube is shown in Fig. 2. The solid line shows scattering from the dense sediment at the bottom of the tube, and is equivalent to a powder diffraction pattern of the clay superimposed on the glass/water background. Scans taken through a gel region in the middle of the tube (circles), where the sample is viscous and cloudy, are identical on the scale of this figure to the scattering from pure water (not shown), except for the intense (001) Bragg peak. The dashed line shows the contribution from empty glass. The bulk water background is reduced by 75% in the sediment relative to the gel region, implying that the clay occupies about 25% of the volume in the sediment.

The $(HK0)$ peaks, such as the (020) peak labeled in Fig. 2, have an asymmetrical shape characteristic of clay particles with disorder in the layer plane [22]. These peaks are sharper than the basal peaks, and are broadened by the resolution chosen for this study. Since no crystallographic refinements of this clay are yet available, and because the present study has a limited q range and a very large background, we do not attempt here to determine the structure factor that produces these lineshapes.

The $(00L)$ peaks are well fit by a Lorentzian line shape, as shown in the inset of Fig. 3 for a two-theta scan of the (001) peak in a sediment layer (open circles). The instrumental resolution was optimized for this (001) peak by narrowing the detector slits until no peak broadening was apparent, and then further closing them by a factor of 2. In the analysis that follows, the $(00L)$ peaks are characterized by Lorentzian fits with a linear background. Because the scattering angles are small, no corrections were made for the slight differences in x-ray intensity or absorption that could arise from variations in tube widths or path length of the beam through the water. No corrections for instrumental broadening have been applied to the data. Polarization of the synchrotron beam, which leads to a factor of 0.95 for the largest scattering angle of $2\theta = 12.5$, has also been ignored.

The narrowest (001) peaks have a Lorentzian full width at half maximum of $\Delta(2\theta) = 0.023° = 0.4$ mrad or $\Delta q = 0.004$ Å^{-1}. We estimate the clay particle thickness as $2\pi/\Delta q = 1600$ Å, identical to our observations for dry powders and pressed samples [19,20]. Among the regions studied, some have (001) peaks that are broader than this by a factor of 4 or so, which we interpret as the segregation of smaller particles (minimum thickness ≈ 400 Å) into those strata. We also find a slight broadening of the higher order peaks, which may be an effect of particle size polydispersity or of strain. The roughly linear dependence of peak width on $\sin\theta$ for the (001), (002), and (003) peaks of various samples, shown in Fig. 3, is consistent with a strain $\Delta c/c \approx 1.5\%$ [23]. Further measurements will be required to make stronger statements about the effects of strain and particle size in this system.

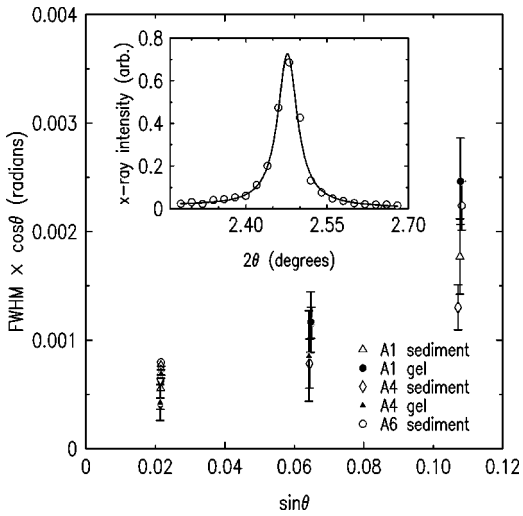

FIG. 3. Williamson-Hall analysis based on Lorentzian full widths at half maximum of (00L) peaks for several layers. Labels A1, A4, and A6 refer to NaCl concentrations of 1.3×10^{-2},8.0×10^{-3}, and $1.0\times10^{-3}M$ respectively. Inset: typical (001) peak (○) with Lorentzian fit (—).

We find that the (001) peak always appears at 0.42 Å^{-1}, corresponding to a c lattice constant of 15.0 Å. This is the largest of three c lattice constants observed so far for Na fluorohectorite, which when dried at high temperatures has $c = 9.7$ Å, and can also be hydrated under cooler and more humid conditions into states having $c = 12.4$ and 15.0 Å [11,19,20]. Taken together, our observations on the peak positions and widths tell us that the particles in solution are composed of well crystallized stacks of 20–100 of the fundamental silicate lamellae. Even when dispersed in water, this clay has no ability to hydrate further or to exfoliate in the solution, at any NaCl concentration investigated here. This behavior is probably due to the large intrinsic layer charge of Na-Fh, which does not permit further separation of the silicate layers from the intercalated cation.

B. Scattering geometry and particle reorientation

By comparing intensity measured in the two different scattering geometries, we can see that particle orientation as well as density changes as a function of height in the tube. In Fig. 4, we show raw intensities at the (001) peak position as a function of sample height, in a tube having three strata discernible by eye. The top curves present a time series taken over 13.5 h, with the spectrometer aligned to scattering in the

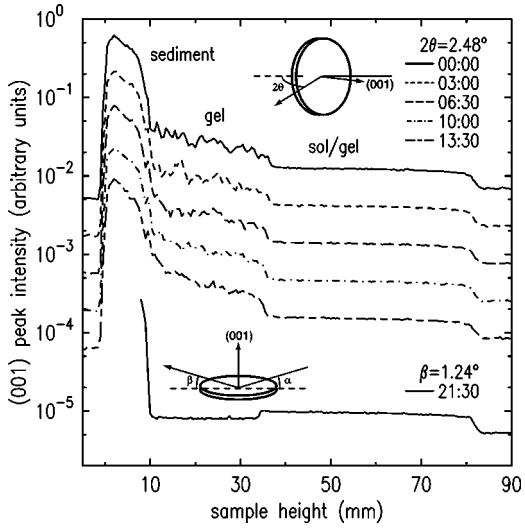

FIG. 4. Intensity at the (001) peak position as a function of beam position in the tube (data are shifted for clarity), for sample with $1.0\times10^{-3}M$ NaCl. Top series: time dependence of peak in $q_{\|}$ showing density variation with height as the sample settles and gels. Bottom curve: peak in $q_{\perp}$ demonstrating the reorientation of the clay particles (see text). Insets illustrate the relationship between particle orientation and scattering geometry.

horizontal plane ($\alpha=\beta=0,2\theta=2.48°$). The resulting intensity comes from that subset of vertical particles that have the correct azimuthal orientation (Fig. 4, inset at top). The zero position of sample height is set at the rounded end of the tube, which is uniform in width above 6 mm or so. The intensity drops by an order of magnitude from the dense sediment ($z<10$ mm) to the gel region just above it ($10<z<36$ mm), and drops again to near-background levels in a third sol/gel layer ($36<z<80$ mm). These designations refer to the sample appearance, which goes from a powdery sediment at the bottom, to a very viscous cloudy region, and to a translucent white liquid above, that became viscous after about a week. The intensity variations on the scale of millimeter in the gel persist over tens or hundreds of minutes, and are apparently due to density variations in the gel as it relaxes. A sample height scan configured for horizontal platelets is shown in the bottom curve ($\alpha=\beta=1.24°,2\theta=0$). The same boundaries in sample height are present, but instead of a monotonic decrease in intensity with sample height, an increased intensity is found going from the middle layer to the top layer. This is direct evidence of particle reorientation: while the density in the top layer may indeed be lower than that of the middle one, the absolute number of horizontal platelets, with their (001) axes aligned perpendicular to the strata, has nevertheless increased there.

IV. ANALYSIS

By fitting background-subtracted (001) peaks in the two scattering configurations, we can assess the relative populations of horizontal and vertical platelets as a function of sample height. It is important to emphasize an essential difference between the two scattering geometries. The intensity found at the (001) position in $q_{\perp}$ will be proportional to all particles that are horizontal (the c axis must be aligned within 0.1 degrees to the momentum transfer, to scatter into our resolution volume). The (001) intensity in $q_{\|}$ is proportional only to those vertical particles whose (001) axes have the correct azimuthal orientation, as the inset of Fig. 4 suggests. We, particularly, want to note a kind of deceptive asymmetry in the use of the words ''horizontal'' and ''vertical.'' The phrase ''vertical particles'' would ordinarily apply to the entire set of azimuthal orientations [for example, imagine their (001) Bragg peaks distributed along all points of an equatorial ring]. It is very important to note that our two scattering configurations probe equal fractions of the possible particle orientations. ''All'' of the horizontal particles have (001) reflections that point straight up into a small resolution volume. A ''small fraction'' of the vertical particles have (001) axes pointing in a particular direction in the horizontal plane, into an equal resolution volume. While it is possible that particles in the gel regions have a preferred azimuthal orientation, this was not investigated experimentally. In future work, it will be advisable to integrate over the vertical particles with a rotation of the sample, as well as perhaps to devise a less confusing nomenclature.

The orientational anisotropy depends strongly on the salt concentration. Figure 5 shows integrated (001) peak intensities (top panels) and full widths at half maximum (bottom panels) for four different NaCl concentrations. The vertical dashed lines separate sediment, gel, sol/gel, and ''water'' strata as discerned by eye. ''Water'' refers to a clear solution in which clay Bragg peaks were generally too weak to be distinguished from the background. The label ''vertical platelets'' (open circles) refers to (001) intensity scattered in the horizontal plane and measured as a function of $q_{\|}$. The (001) peak of a ''horizontal platelet'' (closed circles) is characterized by scanning $q_{\perp}$. Measurements of the (020) peaks at the same sample heights showed qualitatively similar orientation dependence.

Differences in integrated intensity are due to the combined effects of density and particle orientation. In principle, x-ray analysis can be used to obtain both the density and the particle orientation of these clay gels. Unfortunately, independent measurement of the density of the clay suspensions was not possible to obtain either by x-ray absorption or by scattering under the present experimental conditions. Generally, absorption is dominated by the water. For the sediment at the bottoms of the tubes, irregularities in the glass, which has approximately the same mass absorption coefficient as the clay, made quantitative assessment impossible. Since the structure factor of this clay is not yet known, measured peak intensities cannot be directly related to the density. Qualitatively, we can see that the intensity from horizontal platelets makes a relatively large contribution in the sediments, drops markedly in the gels, and in some cases increases again in the sol/gel regions.

The simplest quantitative relationship between the two scattering configurations is the case of an isotropic phase, exemplified by the sol/gel regions in Figs. 5(a) and 5(b). Here, all particle orientations are equally probable and, therefore, the scattered intensity will not depend upon the direc-

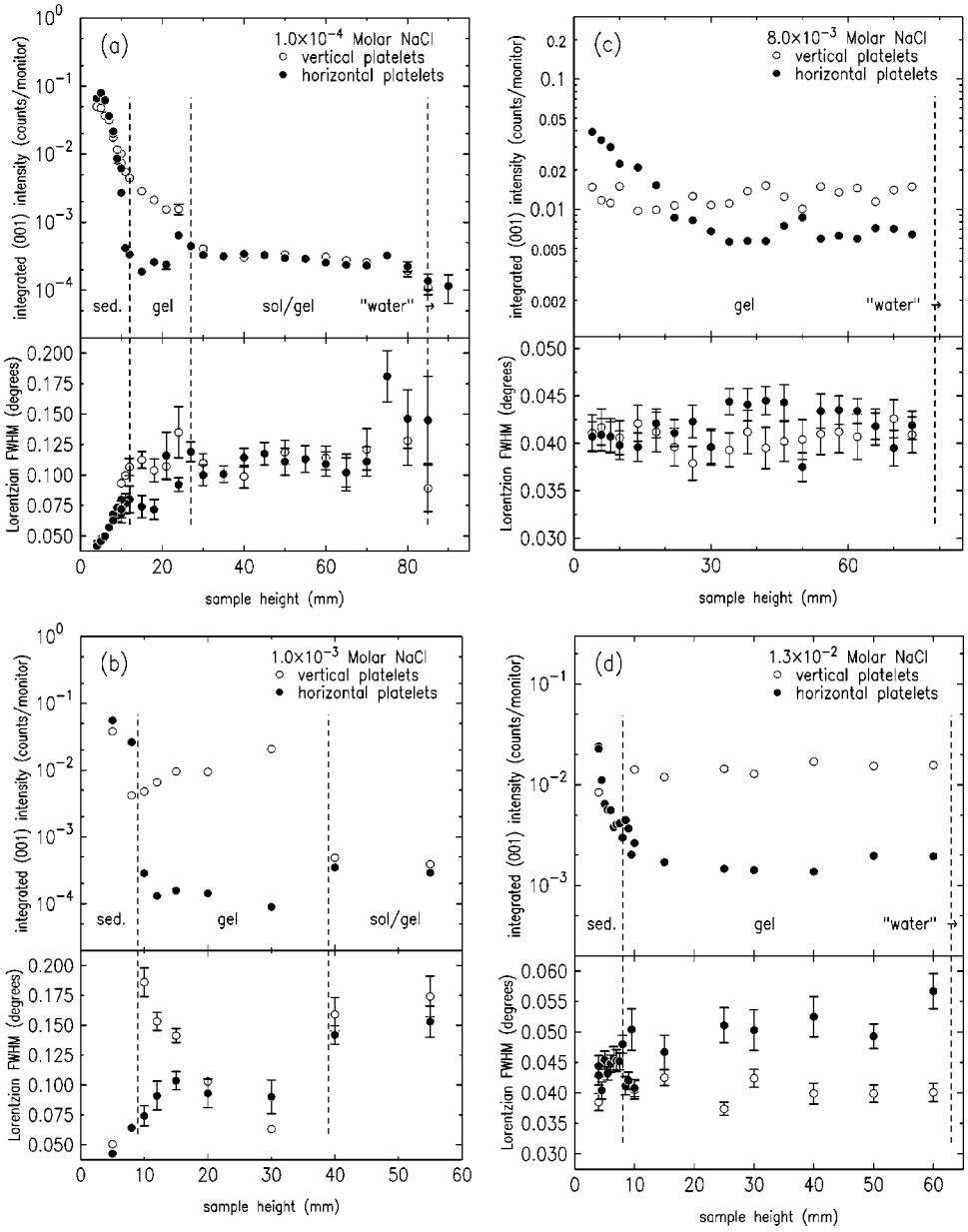

FIG. 5. Top panels: intensities of (001) peaks coming from vertical and horizontal platelets. Lower panels: Lorentzian peak full widths at half maximum. Vertical dashed lines show boundaries identifiable by eye in the sample tubes. (a) $1.0\times10^{-4}M$ NaCl, 2.91 wt.% clay. (b) $1.0\times10^{-3}M$ NaCl, 2.98 wt.% clay. (c) $8.0\times10^{-3}M$ NaCl, 2.93 wt.% clay. (d) $1.3\times10^{-2}M$ NaCl, 2.91 wt.% clay.

tion of the momentum transfer. Intensities as functions of $q_{\parallel}$ and $q_{\perp}$ are equal, as expected. In the sediments, the samples also appear to be essentially isotropic, with a slight tendency towards predominance of horizontal particles at the bottom.

In the gels, differences in the two sets of measured intensities clearly show that the samples are anisotropic. Ratios of the scattered intensity from vertical vs horizontal particles in the gels of Fig. 5(a), 5(b), and 5(d) range from 10 to 100. As we remarked above, it is very likely that we are scattering from only a tiny fraction of the vertical particles, since we are sensitive to only those with the correct azimuthal orientation. Thus, the measured anisotropies of 10–100 are only a lower bound and the real anisotropy may be several orders of magnitude greater. Thus, the gel regions of these three samples are composed almost entirely of vertical platelets, with a rather uniform distribution. This orientational anisotropy is required for nematic order, though not strictly equivalent with it. In principle our data are also consistent with particles that are aligned with their planes in the gravitational field, but are not necessarily parallel to their neighbors. We regard the nematic order as the correct explanation, however. Interactions with the tube walls are presumably responsible for the overall vertical alignment. The gel region of Fig. 5(c) appears to be different from those of the other three samples. The intensity ratios are always less than a factor of 5, becoming less than unity towards the tube bottom. In this case, aligned domains may persist over much shorter length scales, coexisting with others oriented along different directions.

From the plotted peak widths, we can observe changes in the typical particle thickness among the strata. First, we see that the bottoms of the sediments are always composed of the thickest particles [those having the narrowest (001) peaks of $\approx 0.04°$]. The particles in suspension at low salt concentrations are significantly thinner, with peaks broader by factors of two to four [Figs. 5(a) and 5(b)]. By contrast, at higher salt concentrations, the thickest particles occur in the

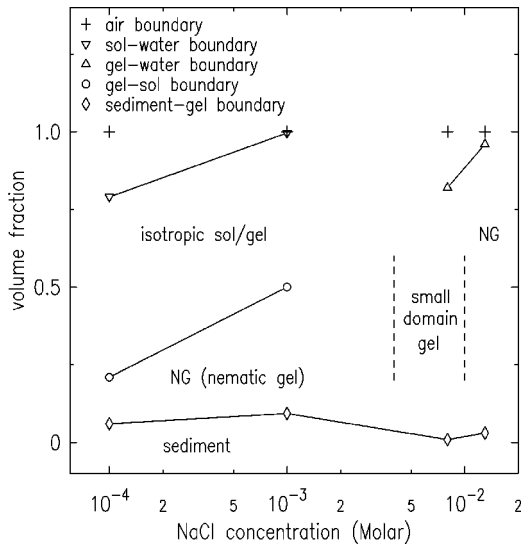

FIG. 6. Phase diagram relating vertical positions of phase boundaries to NaCl concentration. Heights have been converted to relative volumes taking the varying tube diameters into account. Lines are guides for the eye.

gel regions. We find no systematic dependence of particle thickness with orientation.

V. DISCUSSION

The phase diagram of Fig. 6 summarizes the relationship between NaCl concentration and vertical positions of phase boundaries. Heights have been converted to relative sample volumes by taking the tube widths (which vary from 6.5 to 9.5 mm) into account. The sediment, nematic, and isotropic regions are identified clearly, and obviously depend strongly on NaCl concentration. As we remarked above, our measurements were made within a week or two of the sample preparation, while reports on other clay gel systems report dynamic processes continuing over months or even years [24]. After five months' further settling time our samples had changed substantially: to the eye, one or two gels occupied very small volumes above the sediments, with large regions of clear supernatant liquid. Since the volumes occupied by each phase are determined by the speed of gellation or flocculation, we can understand the absence of the isotropic sol/gel in the salt-rich regions of Fig. 5(c) and 5(d). Here the high ionic concentration leads to more rapid settling, just as similar NaCl concentrations of 0.01–0.1M were found to flocculate solutions of bentonite and laponite, clays that form gels when the NaCl concentration is lower [3,4,8]. Nowhere in the Na-Fh/NaCl system do we find a stable isotropic gel, and this is further evidence against the ''house of cards'' model.

Our scattering measurements reveal information complementary to other techniques, especially as regards the nematic gel. Previous identification of nematic order has relied upon optical observations of birefringence through crossed polarizers [3]. In such observations, some assessment can be made of domain sizes (if they are large enough) and alignments. It is notable, however, that in the presence of many small domains there may be a net cancellation of birefringence. Furthermore, optical observations are frequently prevented by opacity in colloidal systems [25,26]. By contrast, the x-ray measurements average over the entire sample illuminated by the beam. As a result, we can asses the overall uniformity of the anisotropic gel regions in Figs. 5(a), 5(b), and 5(d) and the rather different behavior of the ''small domain gel'' of Fig. 5(c) with its smaller and position-dependent anisotropy. The orientationally-sensitive Bragg scattering we present here also provides complementary information to small-angle scattering. The layers and columns of smectic or columnar liquid crystals produce peaks at small scattering angles, [17,25,26] while the Bragg technique cannot distinguish between these phases and the nematic one. However, the nematic phase is positionally disordered and has no clear signature at small scattering angles, but is readily identified in the present measurements.

Since the stability of various types of liquid crystalline order depends upon the size dispersity, it is important in polydisperse systems to find out the extent to which different sizes are segregated in the solution. A strength of the present study is the direct *in situ* measurement of the particle thickness, as estimated from the (001) peak widths. Our data show that the particles stabilized in the anisotropic gels at low NaCl concentrations [Figs. 5(a) and 5(b), lower panels] are, on average, thinner and more polydisperse than those in the salt-rich gels [Figs. 5(c) and 5(d)]. Since the high- and low-salt regions are separated by the ''small-domain'' gel that is apparently much less anisotropic than those elsewhere in the phase diagram, we might speculate that a delicate balance exists between ionic strength and particle size in this region. At present, we do not know how the plates' diameters scale with thickness, so it is not clear whether a change in particle anisotropy plays a role here. To address this and other questions in the present tantalizingly incomplete phase diagram, a high-resolution study of the ($HK0$) peaks is planned, in combination with further crystallographic, small-angle scattering, and microscopy studies.

VI. SUMMARY

We have studied gravity-dispersed phases in suspensions of the synthetic clay Na fluorohectorite in aqueous solutions of $10^{-4}-10^{-2}M$ NaCl. Two distinct anisotropic gel regions have been identified. One is a nematic gel in which most particles are aligned vertically, and the resulting orientational anisotropy is uniform throughout the whole extent of the layer. The second gel is characterized by a small and nonuniform anisotropy in particle orientation, suggesting the presence of smaller aligned domains. Higher NaCl concentrations were found to have two clear effects. An isotropic, slowly gelling suspension was stable over two weeks at 10^{-4} and $10^{-3}M$ NaCl, while at 8×10^{-3} and $1.3\times10^{-2}M$ NaCl rapid flocculation of this layer occurred. Also at higher NaCl concentrations the gels were composed of thicker and more monodisperse particles. No evidence was found for stable, isotropic gels composed of aggregates having the ''house of cards'' structure. Further investigation of the system and the particle morphology is underway.

ACKNOWLEDGMENTS

We appreciate discussions with B. Noheda and T. Vogt at Brookhaven National Laboratory. J.O.F acknowledges the Norwegian Research Council (NFR) for financial support. The CMC beamline is supported in part by the USDOE Office of Basic Energy Sciences and NSF-DMR. The Advanced Photon Source is supported under USDOE Contract No. W-31-109-Eng-38. Preliminary studies performed at beamline X22A at the National Synchrotron Light Source were supported under USDOE Contract No. DE-AC02-98CH10886.

[1] H. van Olphen, *An Introduction to Clay Colloid Chemistry* (Interscience, New York, 1977).
[2] S. A. Solin, in *Chemical Physics of Intercalation II*, edited by P. Bernier *et al.* (Plenum Press, New York, 1993), p. 161.
[3] J.-C. P. Gabriel, C. Sanchez, and P. Davidson, J. Phys. Chem. **100**, 11139 (1996).
[4] A. Mourchid, E. Lécolier, H. van Damme, and P. Levitz, Langmuir **14**, 4718 (1998).
[5] M. Dijkstra, J.-P. Hansen, and P.A. Madden, Phys. Rev. E **55**, 3044 (1997).
[6] L. Onsager, Ann. N.Y. Acad. Sci. **51**, 627 (1949).
[7] R. Eppenga and D. Frenkel, Mol. Phys. **52**, 1303 (1984).
[8] A. Mourchid, A. Delville, J. Lambard, E. Lécolier, and P. Levitz, Langmuir **11**, 1942 (1995).
[9] M. Kroon, G.H. Wegdam, and R. Sprik, Phys. Rev. E **54**, 6541 (1996).
[10] J.D.F. Ramsay and P. Lindner, J. Chem. Soc., Faraday Trans. **89**, 4207 (1993).
[11] P.D. Kaviratna, T.J. Pinnavaia, and P.A. Schroeder, J. Phys. Chem. Solids **57**, 1897 (1996) .
[12] J.O. Fossum, Physica A **270**, 270 (1999).
[13] J. O. Fossum, in *Soft Condensed Matter: Configurations, Dynamics and Functionality*, Vol. 552 of *NATO Advanced Study Institute Series C Mathmetical and Physical Sciences*, edited by A. T. Skjeltorp and S. F. Edwards (Kluwer Academic Publications, Dordrecht, The Netherlands, 2000).
[14] M.A. Bates and D. Frenkel, J. Chem. Phys. **110**, 6553 (1999).
[15] M.A. Bates, J. Chem. Phys. **111**, 1732 (1999).
[16] F.M. van der Kooij, A.P. Philipse, and J.K.G. Dhont, Langmuir **16**, 5317 (2000).
[17] F.M. van der Kooij, K. Kassapidou, and H.N.W. Lekkerkerker, Nature (London) **406**, 868 (2000).
[18] A good, recent review of liquid surface scattering methods and applications can be found in Synchrotron Radiat. News: **12** (1999).
[19] B Noheda (unpublished).
[20] G. J. da Silva, J. O. Fossum, and E. DiMasi (unpublished).
[21] Corning Incorporated, Corning, NY 14831.
[22] R. C. Reynolds, in *Modern Powder Diffraction*, edited by D. L. Bish and J. E. Post, Reviews in Mineralogy (BookCrafters, Chelsea, Michigan, 1989), Vol. 20, p. 147.
[23] G.K. Williamson and W.H. Hall, Acta Metall. **1**, 22 (1953).
[24] A. Mourchid and P. Levitz, Phys. Rev. E **57**, R4887 (1998).
[25] A.B.D. Brown, S.M. Clarke, and A.R. Rennie, Langmuir **14**, 3129 (1998).
[26] A.B.D. Brown, C. Ferrero, T. Narayanan, and A.R. Rennie, Eur. Phys. J. B **11**, 481 (1999).